Binding Mechanisms of PEGylated Ligands Reveal Multiple Effects of the PEG Scaffold†

Raibatak Das,‡,§ Emily Baird,‡,|| Scott Allen,‡ Barbara Baird,‡ David Holowka,‡ and Byron Goldstein*,⊥

Department of Chemistry and Chemical Biology, Cornell University, Ithaca, New York 14853-1301, and Theoretical Biology and Biophysics Group, T-10 MS K710, Los Alamos National Laboratory, Los Alamos, New Mexico 87545

Received October 17, 2007; Revised Manuscript Received November 12, 2007

ABSTRACT: A series of synthetic ligands consisting of poly(ethylene glycol) (PEG), capped on one or both ends with the hapten 2,4-dinitrophenyl (DNP), were previously shown to be potent inhibitors of cellular activation in RBL mast cells stimulated by a multivalent antigen [Baird, E. J., Holowka, D., Coates, G. W., and Baird, B. (2003) *Biochemistry 42*, 12739−12748]. In this study, we systematically investigated the effect of increasing length of the PEG scaffold on the binding of these monovalent and bivalent ligands to anti-DNP IgE in solution. Our analysis reveals evidence for an energetically favorable interaction between two monovalent ligands bound to the same receptor, when the PEG molecular mass exceeds ∼5 kDa. Additionally, for ligands with much higher molecular masses (>10 kDa PEG), the binding of a single ligand apparently leads to a steric exclusion of the second binding site by the bulky PEG scaffold. These results are further corroborated by data from an alternate fluorescence-based assay that we developed to quantify the capacity of these ligands to displace a small hapten bound to IgE. This new assay monitors the displacement of a small, receptor-bound hapten by a competitive monovalent ligand and thus quantifies the competitive inhibition offered by a monovalent ligand. We also show that, for bivalent ligands, inhibitory capacity is correlated with the capacity to form effective intramolecular cross-links with IgE.

In many biological signaling systems, the cross-linking of cell surface receptors by a multivalent ligand initiates an intracellular response (*1*). A well-studied example is the allergic immune response elicited by a multivalent antigen that cross-links its cognate antibody IgE, bound to the high-affinity receptor FcϵRI, on the surface of mast cells and basophils. After receptor cross-linking, the Src family kinase Lyn phosphorylates immunoreceptor tyrosine-based activation motifs (ITAMs) in the β and γ subunits of the cross-linked receptor (*2*), and the ensuing signaling cascade leads to the degranulation of these cells, releasing vesicular contents such as histamine that mediate the physiological symptoms of allergies. The requirement of intermolecular receptor cross-linking suggests that a potential strategy for inhibiting this response is to design a monovalent antigen that acts as a competitive inhibitor. It has been shown that monovalent haptens in solution can effect the dissociation of a majority of cell surface-bound multivalent antigen and rapidly terminate the degranulation response (*3*). Another inhibitory strategy relies on an appropriately designed bifunctional ligand whose functional groups are separated by a distance that matches the separation between the two binding sites on an IgE. Such a bivalent ligand is expected to form preferentially a nonactivating intramolecular cross-link between the two binding sites and thus function as a high-avidity inhibitor of a multivalent antigen.

In a previous paper from our laboratory, Baird et al. (*4*) demonstrated the potential of one such class of specific inhibitors in an in vitro model system. The authors synthesized a series of ligands consisting of poly(ethylene glycol) (PEG)[1] functionalized with a DNP group on one end (MeO−PEG_x−DNP) or both ends (DNP−PEG_x−DNP). PEG was chosen as the molecular scaffold because of its excellent biocompatibility, minimal nonspecific interactions, and numerous successful biomedical applications (*5*). These ligands were shown to be potent inhibitors of the degranulation response induced by the multivalent antigen DNP-BSA in RBL-2H3 mast cells sensitized with anti-DNP IgE. The inhibitory capacity was quantified by measuring their IC_{50} values, defined here as the concentration of a ligand that inhibits 50% of the degranulation stimulated by an optimal dose of DNP-BSA. These measurements revealed a significant influence of the PEG scaffold on the inhibitory capacity.

† This work was supported by the Cornell Nanobiotechnology Center, an STC Program of the NSF (ECS-9876771), Dept. of Energy through contract W-7405-ENG-36, and NIH Grants R37-GM035556 and R01-AI22449.

* To whom correspondence should be addressed. Phone: (505) 667-6538. Fax: (505) 665-3493. E-mail: bxg@lanl.gov.

‡ Cornell University.

§ Current address: Department of Mathematics, University of British Columbia, 1984 Mathematics Rd., Vancouver, BC, Canada V6T 1Z2.

|| Current address: University of Pennsylvania School of Medicine, Philadelphia, PA 19104.

⊥ Los Alamos National Laboratory.

[1] Abbreviations: BSS, buffered saline solution; DCC, dicyclohexylcarbodiimide; DCT, {ϵ-[(2,4-dinitrophenyl)amino]caproyl}-L-tyrosine; $(DCT)_2$-cys, *N*,*N*′-bis({ϵ-[(2,4-dinitrophenyl)amino]caproyl}-L-tyrosyl)-L-cystine; DMAP, 4-(dimethylamino)pyridine; DNP, 2,4-dinitrophenyl; DNP-BSA, bovine serum albumin multiply conjugated with DNP; FITC, fluorescein isothiocyanate; PEG, poly(ethylene glycol); TEA, triethylamine.

10.1021/bi702094j CCC: $40.75
Published on Web 12/23/2007

Baird et al. (*4*) noted that for monovalent ligands, the inhibitory capacity generally increased with the PEG molecular mass.

Why does the PEG tether affect the inhibitory capacity of these ligands? It is known that tethering PEG to a surface results in a steric stabilization that repels other macromolecules (*6*). By analogy, we reasoned that when a monovalent ligand is bound to an IgE, the bulky PEG tether blocks the approach of a multivalent antigen. Therefore, a *prima facie* explanation for the observed trend in inhibitory capacity is that this steric effect becomes more pronounced with an increase in PEG molecular mass. If this is indeed the correct inhibitory mechanism, then a monovalent ligand bound to one of the sites on an IgE is also expected to inhibit the approach of a second monovalent ligand to the other binding site on the same IgE, resulting in a lower apparent affinity for the ligand−IgE interaction. Detailed kinetic measurements using BIAcore have demonstrated a reduced apparent affinity of an antibody fragment conjugated to a 20 kDa PEG for surface-immobilized binding sites (*7*). The reduction was attributed to a lowered rate of association for the binding due to a steric blockage of the binding sites by the large PEG tether. We similarly expected the higher-molecular mass ligands to exhibit a lower apparent affinity for IgE in conjunction with a lower IC_{50}. On the contrary, MeO−PEG_{5000}−DNP, the longest monovalent ligand examined in the previous study, showed both an unusually high inhibitory capacity and a high apparent affinity for anti-DNP IgE in solution (*4*). This contradictory observation led us to examine in greater detail the binding interaction between monovalent PEG ligands and IgE.

In this study, we used a fluorescence assay to quantify the binding of monovalent PEG ligands to IgE in solution. We fit the binding data to two different binding models: one which treats the two binding sites on an IgE as independent and having identical affinity for a monovalent ligand and another in which the affinity for a binding site is influenced by whether the second site on that IgE is free or occupied. The first model assumes no interaction between two ligands bound to the same IgE, and the second model allows such an interaction to increase or decrease the overall (effective) affinity of the ligand for IgE. We systematically analyzed the binding data for ligands with a range of PEG molecular masses from 350 Da to 20 kDa. Our results point to an energetically favorable interaction between two monovalent ligands bound to the same IgE when the PEG molecular mass exceeds 5 kDa.

Baird et al. (*4*) also showed that the length of the PEG spacer determines the effectiveness of a bivalent ligand as an inhibitor. The capacity of a bivalent ligand with an appropriate length spacer to form efficient intramolecular cross-links has also been utilized to design stimulators of proteins with multiple binding sites as reported by Kramer and Karpen (*8*). These authors showed that optimal length PEG-linked dimers were potent allosteric activators of a variety of multisubunit proteins, bound with unusually high affinities to their target, and dissociated slowly even in the presence of a monovalent competitor in solution. Baird et al. similarly observed a correlation between inhibitory capacities and lengths of the PEG scaffolds for bivalent ligands. Shorter ligands with a PEG molecular mass of ≤1 kDa (solution length of 28 Å, extended length of 110 Å) were relatively modest inhibitors, while longer ones with a PEG molecular mass of ≥3350 Da (solution length of 52 Å, extended length of 290 Å) were potent inhibitors with IC_{50} values approaching ≤10 nM (*4*). In this study, we also analyzed the binding interaction between bivalent ligands and IgE in solution with a binding model that takes into account the formation of intramolecular cross-links. Our analysis of the solution binding data reveals a strong correlation between the intramolecular cross-linking constant and the inhibitory capacity.

MATERIALS AND METHODS

Synthesis and Purification of MeO−PEG_{10000}−DNP and MeO−PEG_{20000}−DNP. The synthesis and purification of MeO−PEG_{10000}−DNP and MeO−PEG_{20000}−DNP [(*N*-2,4-DNP-ϵ-amino caproate)−*x*MPEG] were carried out as previously described (*4*). All solvents and reagents were ordered from Aldrich and used as received unless otherwise noted. Gel permeation chromatography was performed using Bio-Beads S-X1 beads (200−400 mesh, Bio-Rad). Poly(ethylene glycol)s (Rapp Polymere Gmbh) of different polymer weights (PEG_x), and with a polydispersity of less than 1.05, were dried under vacuum for 4 h at 50 °C. To a solution of PEG (0.02 mmol) in 2 mL of methylene chloride were added *N*-2,4-DNP-ϵ-aminocaproic acid (0.05 mmol), dicyclohexylcarbodiimide (DCC) (0.03 mmol), and 4-(dimethylamino)-pyridine (DMAP) (0.002 mmol). The reaction mixture was stirred at room temperature for 12 h under nitrogen. The mixture was filtered, and the solvent was removed via rotary evaporation. The yellow residue was dissolved in a minimum amount of THF and purified by gel permeation chromatography using THF as the eluent. ^{1}H NMR spectra were recorded on a Varian 500 MHz spectrometer; chemical shifts are reported relative to residual protonated solvent. Physical characteristics and spectral information for the two compounds are detailed in the Supporting Information.

Equilibrium Binding of PEG Ligands to Fluoresceinated IgE or Fab′ Fragments. Purification and characterization of FITC-anti-DNP-IgE and its monovalent fragement FITC-Fab′ were carried out as previously described (*9*). Specific binding of DNP-capped PEG ligands to fluorescein isothiocyanate (FITC)-modified anti-DNP IgE or its Fab′ fragment was monitored by a fluorescence quenching assay described previously (*10*). Fluorescence measurements were carried out on an SLM 8100 fluorescence spectrophotometer in time-series acquisition mode. For each experiment, FITC-IgE (or FITC-Fab′) in 2 mL of a buffered saline solution (BSS) containing 1 mg/mL gelatin (20 mM Hepes, 135 mM NaCl, 5 mM KCl, 1.8 mM $CaCl_2$, 1 mM $MgCl_2$, and 5.6 mM glucose adjusted to pH 7.4) was stirred continuously in an acrylic cuvette. Fluorescein was excited at 490 nm, and the emission was recorded at 520 nm. Indicated concentrations of PEG ligands were added sequentially, and the fluorescence was recorded to monitor the specific binding to IgE. The effective concentrations of anti-DNP binding sites in these titrations were determined from titrations with the high-affinity monovalent ligand, DCT, as previously described (*10*).

Analysis of Equilibrium Binding Data. Data from the binding titrations between the PEG ligands and IgE in solution were fit to different equilibrium binding models

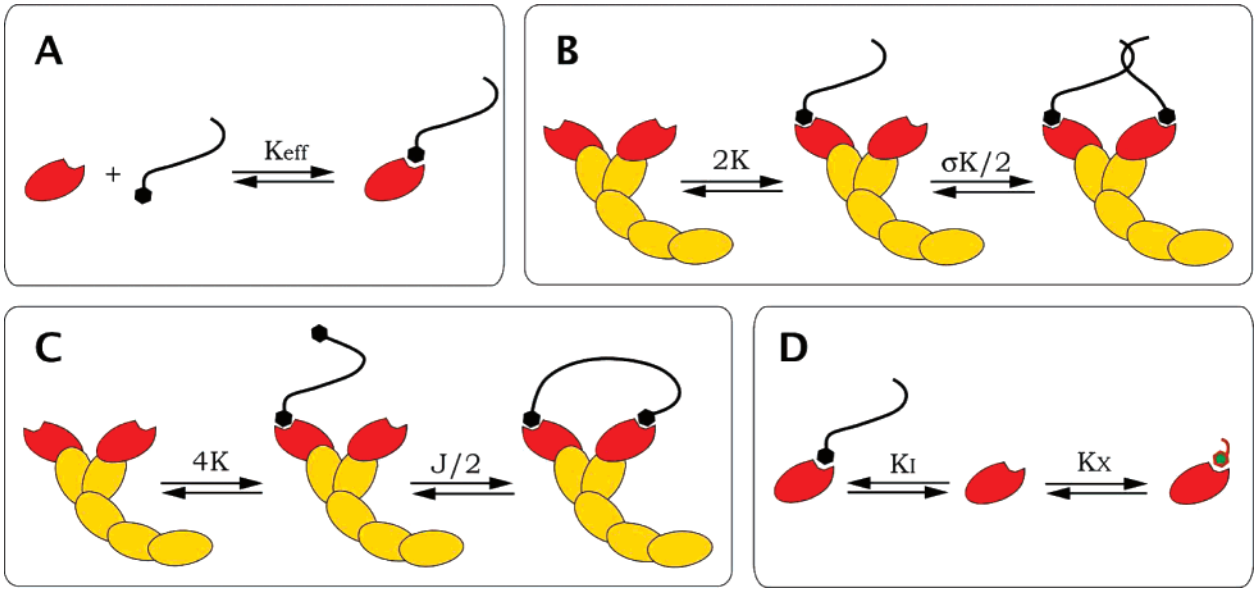

FIGURE 1: Schematic illustrations of the models used for fitting direct and competitive binding data. (A) In the single-step binding model, each binding site on an IgE is assumed to bind a ligand independently and with an identical affinity K_{eff}. (B) In the two-step binding model, two monovalent ligands sequentially bind to an IgE with different affinities. (C) In the bivalent binding model, one functional group on a bivalent ligand first binds to a free IgE, and the singly bound complex then isomerizes to an intramolecularly cross-linked state. (D) In the competitive binding model, a monovalent ligand and a small fluorescent hapten compete with different affinities for the binding sites on a receptor. See the Appendix for more details and the equations derived from each model.

schematically shown in Figure 1. We first used a single-step binding model (Figure 1A) to determine the effective affinity between the DNP group on a ligand and the binding site on an IgE (or Fab′). Additionally, to model the binding of monovalent ligands to IgE, we used a more realistic two-step binding model (Figure 1B) in which an IgE binds two monovalent ligands with different affinities. For bivalent ligands, we used a model that allows the formation of an intramolecular cross-link following the initial binding (Figure 1C).

Each model is parametrized by a set of equilibrium constants for the transformations of an antibody between its unbound and various bound forms. In the Appendix, we derive equations that express the fraction of antibody binding sites that are occupied (f) as a function of the total ligand concentration (L_T), the total receptor concentration (R_T), and the equilibrium constants for each of these models. As described in detail in the Supporting Information, we used nonlinear least-squares regression to estimate best-fit parameter values and established bootstrap confidence intervals for these parameter estimates (*11*).

Synthesis and Characterization of the Hapten DNP-Lys-Flu for Competitive Inhibition. A 4:1 mixture of Nϵ-(2,4-dinitrophenyl)-L-lysine hydrochloride (DNP-Lys; Sigma) and 6-(fluorescein-5-carboxamido)hexanoic acid, succinimidyl ester (5-SFX; Molecular Probes) (~20 mM DNP-Lys and ~5 mM 5-SFX) in 10 mM aqueous triethylamine (TEA) was incubated for 3 h at room temperature (Scheme 1). The reaction mixture was purified using a Waters Symmetry 5 μm C_{18} column (model WAT045905, Waters Corp., Milford, MA) on a Waters HPLC system by eluting with a linear gradient uniformly increasing from 5% aqueous acetonitrile to 25% aqueous acetonitrile over 20 min. Fractions corresponding to a single peak with simultaneous absorption at 360 nm (DNP absorption maxima) and 490 nm (fluorescein absorption maxima) were collected.

To assay their binding capacity, we measured the steady-state fluorescence anisotropy of each fraction ($\lambda_{ex} = 490$ nm; $\lambda_{em} = 520$ nm), before and after the addition of a saturating concentration of anti-DNP IgE (*12*). The HPLC fraction with the maximum relative change showed nearly a 4-fold increase in anisotropy following addition of IgE. This fraction was denoted DNP-Lys-Flu and used as the small hapten in competitive binding assays. Concurrent with the increase in its fluorescence anisotropy, the fluorescence intensity of this ligand also increased by approximately 4-fold when it was bound to anti-DNP IgE. Therefore, in the competitive binding assays, we used the change in fluorescence intensity of DNP-Lys-Flu to quantify its binding to IgE. We determined the affinity K_X of this ligand for IgE through a direct binding titration. DNP-Lys-Flu in 2 mL of BSS containing 1 mg/mL gelatin was stirred continuously, and indicated concentrations of unlabeled IgE were titrated in while the fluorescence intensity was recorded. We used the following equation to describe the saturable increase in the DNP-Lys-Flu fluorescence upon addition of IgE:

$$F'_{model} = F'_{low} + f'(F'_{high} - F'_{low}) \quad (1)$$

where f' is the fraction of the hapten that is bound to IgE, F'_{low} the fluorescence in the absence of any IgE, and F'_{high} the fluorescence at a saturating IgE concentration when all the ligand is bound. The titration data were fit to a single-step binding model (analogous to the one in Figure 1A) to determine K_X.

Competitive Binding Assay. Ten microliters of a 3.7 μM stock of DNP-Lys-Flu was added to 2 mL of BSS containing 1 mg/mL gelatin (final concentration of 18.5 nM DNP-Lys-Flu) and excited at 490 nm. The fluorescein fluorescence at 520 nm was continuously monitored. A single initial addition of anti-DNP IgE was followed by specified additions of the monovalent ligand being used as the inhibitor. The fluores-

cence was recorded after each addition to determine the fraction of the hapten bound to IgE.

Analysis of Competitive Inhibition Data. As described in the Appendix, the model used for fitting the competitive inhibition data (Figure 1D) expresses the fraction of bound hapten f' in terms of the total concentrations of IgE, DNP-Lys-Flu, and the monovalent ligand used, and the affinities K_X and K_I of DNP-Lys-Flu and the monovalent ligand, respectively. The experimentally observed fluorescence was fitted to F'_{model} to determine the best-fit value of the inhibitor affinity K_I, with K_X held fixed at the previously determined association constant for binding of DNP-Lys-Flu to IgE.

RESULTS

Equilibrium Binding of Monovalent PEG Ligands to IgE in Solution. Previously, Baird et al. (*4*) reported the synthesis and functional characterization of a class of ligands that consisted of PEG with different molecular masses, functionalized with DNP at one or both ends. These ligands were designed to be potential inhibitors of the degranulation response induced by a multivalent antigen DNP-BSA in RBL-2H3 mast cells, and they were shown to be effective in this capacity to varying degrees. In this study, we systematically analyzed the binding of these ligands to anti-DNP IgE in solution, to improve our understanding of the effect of the PEG scaffold length on the ligand−antibody binding interaction.

We quantified the binding using a previously described fluorescence-based assay that measures the fraction of IgE binding sites occupied for a given ligand concentration (*10*). This assay utilizes the observed quenching of fluorescein fluorescence when a DNP-containing ligand binds to a FITC-conjugated anti-DNP IgE (FITC-IgE). To determine the affinity constant for this binding interaction, we first fit the binding titration data to a simple one-step binding model (Figure 1A) that treats the two binding sites on an IgE as independent and having identical affinity, K_{eff}. This effective affinity averages over any differences in the two binding events due to factors such as cooperative binding or steric exclusion.

In Figure 2A, we plot this effective affinity constant for the range of PEG molecular masses that were examined. Confidence intervals for the parameter estimates are listed in Table S1 (Supporting Information). We note that the effective affinity constants of monovalent PEG ligands for binding anti-DNP IgE in solution range from $\sim 7 \times 10^7$ to 7×10^8 M^{-1} (with most closer to the lower value). It is also obvious from an examination of this plot that the PEG molecular mass affects the affinity constant in a nonmonotonic fashion. In particular, while the three longest ligands with ≥5 kDa PEG bind IgE with an enhanced effective affinity compared to ligands with lower-molecular mass PEG, the largest effective affinity is observed for the ligand with a 10 kDa PEG, but not the one with a 20 kDa PEG.

Remarkably, we observe these differences in effective affinities for ligands with different PEG lengths, though they all contain an identical seven-atom linker adjacent to the DNP group. Since the DNP group along with these linker atoms constitutes the antigenic epitope for the anti-DNP IgE (*10*), the relatively higher effective affinity observed for ligands

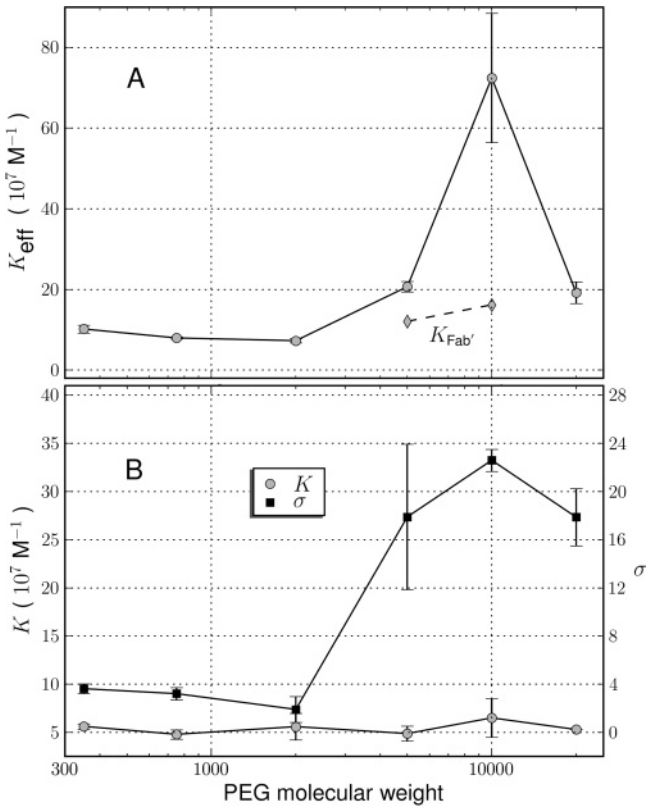

FIGURE 2: Plots of variations in binding parameters of monovalent ligands as a function of the PEG molecular mass. (A) Best-fit values of the effective affinity constant (K_{eff}) determined from fitting the data to the single-step binding model (Figure 1A). Also shown are the binding affinities ($K_{Fab'}$) of the 5 and 10 kDa PEG ligands for monovalent Fab′ fragments. (B) Best-fit values of the intrinsic affinity K and the interaction term σ from fits to the two-step binding model (Figure 1B). For the ligand with 20 kDa PEG, K was fixed at 5.3×10^7 M^{-1} and σ allowed to vary as a free parameter (see the text for details). Note the different scales for K_{eff} and σ in panel B. The best-fit parameter values were determined from simultaneous fits of three to six independent data sets. The error bars shown here are the standard deviations in best-fit values from fits of individual data sets. The fitting procedure is described in the Supporting Information, and Table S1 lists bootstrap confidence intervals for the parameter estimates.

with high-molecular mass (≥5 kDa) PEG points to additional factors that contribute to the effective affinity. One possibility is that the high-molecular mass PEG scaffolds permit interaction between two such ligands held close together, for example, when they are bound to the same IgE. On the basis of the enhanced effective affinity observed for the high-molecular mass ligands, we speculated that this interaction between two high-molecular mass PEG scaffolds confers an additional energetic stability to such configurations. The separation between the two binding sites on an IgE is estimated to be approximately 100 Å based on resonance energy transfer between the two sites (*13*). Therefore, a priori we expect a nominal interaction between two monovalent ligands bound to the same IgE when the solution length of their PEG tails exceeds 50 Å.

To test this hypothesis, we refitted the binding data to a more realistic two-step binding model illustrated in Figure 1B. In this model, two monovalent ligands bind to a bivalent receptor (IgE) sequentially, with different affinities. As described in the Appendix, we parametrize this two-step binding by an intrinsic affinity K and an interaction term σ.

The intrinsic affinity, K, is the affinity constant for the binding of a monovalent ligand to a binding site on an unoccupied receptor. If, however, a binding site on the receptor is already occupied by another ligand, then the binding affinity for a second ligand is σK. Using this notation, a σ of >1 indicates a preference for a doubly bound receptor over two singly bound receptors, and conversely, a σ of <1 indicates that a doubly bound receptor is less energetically favorable compared to two singly bound ones. In this model, the intrinsic affinity K is expected to measure the binding affinity between the antigenic epitope and the IgE binding site and therefore show little dependence on the PEG scaffold length. On the other hand, if, as we hypothesize, the different effective affinities are a consequence of interacting PEG scaffolds, we expect the interaction term σ to differ substantially between two ligands with very different PEG lengths.

The best-fit parameter values of K and σ are plotted in Figure 2B, and confidence intervals for the parameter estimates are listed in Table S1 (Supporting Information). We observe that by fitting the binding data to this two-step binding model we obtain a value for the intrinsic affinity K that indeed shows very little dependence on the PEG molecular mass for ligands with $\leq$10 kDa PEG (see the following section for a discussion of the 20 kDa PEG ligand fit). The relatively small change in K across a broad range of PEG lengths is consistent with our interpretation of K as an intrinsic affinity of the IgE binding site for the antigenic epitope on a ligand. The best-fit value of K from our fits is approximately 5×10^7 M^{-1}, which is somewhat lower than the affinity of the small hapten, DCT, with a more extended antigenic epitope (*10*). This affinity is also comparable to the affinities of another class of macromolecular monovalent DNP ligands consisting of double-stranded DNA modified at its end with DNP and methylene spacers, reported to be in the range of $6-8 \times 10^7$ M^{-1} (*14*). Interestingly, the effective affinity of the dsDNA-DNP ligands reported by Paar et al. showed very little dependence on the length of the dsDNA, which spanned roughly the same length as the solution length of the PEG for the ligands examined here (*14*). The small linker immediately adjacent to the DNP group is identical for the dsDNA ligands and the PEG ligands. Thus, variations in the effective affinity for ligands with high-molecular mass PEG are due to the distinct chemical nature of the PEG scaffold and their flexibility compared to the rigid dsDNA.

Unlike the intrinsic affinity, the interaction term σ shows a strong dependence on the PEG length, and the best-fit values of σ shown in Figure 2B correlate well with the effective binding affinities shown in Figure 2A. We classify the σ values into two distinct regimes based on the PEG scaffold length relative to the estimated separation of 100 Å between the two binding sites on an IgE (*13*). For short ligands with a PEG molecular mass of $\leq$2 kDa, whose solution length is $<$50 Å, σ is close to 1, suggesting that only limited interaction is possible between two ligands bound to the same IgE when the solution lengths of their PEG tails are insufficient to span the distance between the two binding sites. Thus, the presence of a short ligand bound to an IgE binding site does not influence binding at the second site on that IgE.

In contrast, for longer ligands with $\geq$5 kDa PEG, the solution length exceeds 50 Å, permitting an interaction between two ligands bound to the same IgE. For these ligands, σ is at least 1 order of magnitude greater, with a maximum value of $>$20 for the ligand with 10 kDa PEG. These high σ values indicate an energetically favorable conformation when two ligands are bound to the same IgE, which is most likely responsible for their high effective affinity. Our analysis does not reveal a molecular mechanism for the observed stabilization of these intermediate-length PEG ligands. It is possible that in this doubly bound state two PEGs can self-associate or entangle, forming a noncovalent bivalent ligand in situ. These self-associations may be further stabilized in a aqueous buffer by hydrogen bonds between the two PEGs. Such entanglements are either rare or transient between unbound ligands in solution, which is evident from the absence of any detectable receptor cross-linking and mast cell degranulation induced by the ligands alone. However, when two ligands are tethered in close together with separations of $\sim$100 Å, the high local concentration may permit more stable associations.

It is possible that the high values of σ and high effective affinities of these longer ligands arise from nonspecific adhesion between their PEG tethers and IgE. Nonspecific interactions have been previously reported between streptavidin and grafted PEG brushes for 5 kDa PEG (*15*). Because our analysis above does not directly rule out this possibility, we addressed it by examining the binding of the 5 and 10 kDa PEG ligand to monovalent Fab′ fragments of the anti-DNP IgE. Both these ligands have a high effective affinity for IgE in the single-step binding model and a high σ value in the two-step model, compared to those of ligands with shorter ($\leq$2 kDa) PEG. If this enhanced affinity is due to a nonspecific interaction between the PEG scaffolds and IgE, then we expect a similarly high affinity for the binding interaction between these ligands and monovalent Fab′ fragments. We fitted the data from Fab′ titrations to a single-step binding model and determined the affinity of this interaction to be 1.2×10^8 M^{-1} for the 5 kDa PEG ligand and 1.6×10^8 M^{-1} for the 10 kDa PEG ligand (Figure 3 and Table S1). In particular, the much lower affinity for Fab′ compared to the effective affinity for IgE is notable for the 10 kDa PEG ligand.

We observe that the affinities of these ligands for Fab′ are somewhat greater than their corresponding intrinsic affinities for intact IgE (determined by fits to the two-step model) but comparable to the effective affinities of ligands with a shorter ($\leq$2 kDa) PEG tail (determined from fits to the single-step model). Because nonspecific interactions do not lead to a change in the FITC fluorescence, it is not possible to directly determine the contribution of the nonspecific adhesion alone using this simple binding assay. Nonetheless, as shown in the Supporting Information, we can estimate the contribution of nonspecific interactions to binding avidity by assuming that the intrinsic affinity of a ligand for an Fab′ fragment is the same as its intrinsic affinity for an IgE binding site. With this assumption, we estimate that nonspecific interactions with Fab′ enhance the intrinsic affinity by a factor of $\simeq$1.5 for both these ligands. In contrast, σ in the two-step binding model assumes a value more than 10 times greater than this factor of 1.5 for both of these ligands. The parameter σ is a measure of the net enhancement

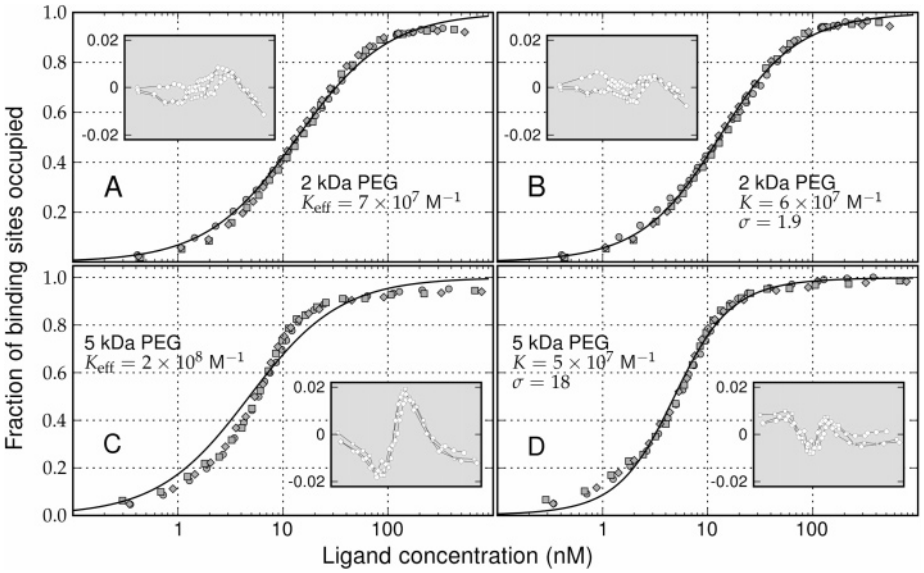

FIGURE 3: Comparison of experimental binding data and their fits to the two binding models for two representative monovalent ligands. The top panels show data for MeO−PEG_{2000}−DNP and the bottom panels for MeO−PEG_{5000}−DNP. For each ligand, experimental data for three independent binding titrations are shown as a scatter plot. The solid lines show the best-fit curves generated by fitting the data to a binding model as follows: (A) MeO−PEG_{2000}−DNP fitted to a single-step binding model (Figure 1A) with a single effective affinity (K_{eff} = 7.3 × 10^7 M^{-1}), (B) MeO−PEG_{2000}−DNP fitted to a two-step binding model (Figure 1B) with a K of 5.6 × 10^7 M^{-1} and a σ of 1.91, (C) MeO−PEG_{5000}−DNP with a K_{eff} of 2.1 × 10^8 M^{-1}, and (D) MeO−PEG_{5000}−DNP with a K of 4.9 × 10^7 M^{-1} and a σ of 17.9. The titration data and the best-fit curve are displayed as a fraction of the IgE binding sites occupied for a given ligand concentration. The insets in each graph show the residuals in the fluorescence values, i.e., the difference between the experimentally observed fluorescence and that predicted by the binding model. The total IgE concentration at the beginning of the titration was 1.6 nM in each experiment shown here.

in binding affinity, with contributions from both nonspecific interactions and positive cooperativity. Thus, these results indicate that while there is a small contribution from nonspecific binding of the PEG tethers to IgE, the high σ values for these ligands are mostly likely due to a positive cooperative interaction between two PEG tails.

Though we classify the ligands into two distinct categories, we note that even for some small ligands (≤2 kDa PEG) the σ values are somewhat higher than 1, consistent with some nonspecific interaction between the PEG tails and IgE, as revealed by our analysis of Fab′ titrations. Additionally, these σ values could also arise from a limited interaction between two short PEG scaffolds on ligands bound to the same IgE. This interaction may be attributed in part to the flexibility in the IgE structure that could bring the two binding sites closer, although IgE is less flexible than IgG (*16*). More likely, the conformational flexibility of PEGs allows them to assume an extended conformation. The solution length (based on a random walk polymer model) and the extended length of PEG for different molecular masses are listed in Table S1, and it is evident that some of the shorter ligands possess sufficient conformational freedom to assume a more extended conformation and interact with another ligand bound to the same IgE. The enthalpic gain from such an interaction likely offsets the entropic loss in assuming the extended conformation.

Alternative Fits for High-Molecular Mass Ligands. In our initial fits of the binding data for the ligand with 20 kDa PEG, by letting both K and σ vary as free parameters, we found a low σ value of ≈0.2 which indicates a steric blockage of the second binding site in the presence of a bound ligand. However, in these fits the parameter K assumed an unreasonably high value that cannot be simply explained by the binding interaction between the antigenic epitope and the binding site. Consequently, we fixed the value of K to be the average of the intrinsic affinity for the shorter ligands and performed the fits by letting only σ vary as a free parameter. With K held fixed at this physically reasonable value, we find the high σ value reported in the previous section (Figure 2B and Table S1). Similarly, for the ligand with 10 kDa PEG, we found another set of best-fit parameter values for which $\sigma < 1$, by using a somewhat different choice of initial guesses to perform the nonlinear regression. Again, this low value of σ is found in conjunction with a nonphysical, high value of K. We did not find such fits of comparable quality but with substantially different best-fit parameter values using different initial parameter guesses for any of the shorter ligands.

The high intrinsic affinity in these fits could arise from nonspecific binding of the long PEG tails to IgE. However, on the basis of our analysis of the binding of 5 and 10 kDa PEG ligands to Fab′, we conclude that such nonspecific interactions contribute little to the enhanced observed binding affinity. Further, as discussed below, an alternate fit, which treats IgE as a monovalent receptor, yields an intrinsic affinity for these long PEG ligands that is comparable to that of shorter PEG ligands. Also, as we show in a later section, the data from a competitive binding assay show no evidence for such nonspecific adhesion that would enhance the intrinsic affinity. Taken together, these results are most consistent with our interpretation that the high intrinsic affinities obtained in these fits are physically unlikely, and not indicative of nonspecific adhesion.

On the other hand, the low σ values in these ersatz fits are consistent with a previously reported steric blockage mechanism mediated by a bulky PEG tether (*7*). In that study, Kubetzko et al. analyzed the binding kinetics between an antibody fragment conjugated to a 20 kDa PEG and surface-immobilized binding sites and concluded that the 20 kDa PEG lowers the effective affinity. The lowered effective

Table 1: Comparison of Fits to a Single-Step Binding Model in Which the IgE Is Treated as Consisting of Two Binding Sites versus a Single Binding Site[a]

ligand	K_{eff} (M^{-1})	$(SS)_{K_{eff}}$	K_{alt} (M^{-1})	$(SS)_{K_{alt}}$
MeO−PEG_{20000}−DNP	1.92×10^8	5.75×10^{-3}	4.25×10^7	7.93×10^{-4}
MeO−PEG_{10000}−DNP	7.25×10^8	1.88×10^{-2}	8.40×10^7	1.19×10^{-3}
MeO−PEG_{750}−DNP	7.98×10^7	5.45×10^{-2}	3.69×10^7	6.17×10^{-3}

[a] K_{eff} is the effective affinity between an IgE binding site and a monovalent ligand when each IgE is treated as consisting of two independent and identical binding sites. K_{alt} is the effective affinity when the IgE is treated as a monovalent receptor capable of binding only one ligand. $(SS)_{K_{eff}}$ and $(SS)_{K_{alt}}$ are the sums of squared residuals from the respective fits. A smaller sum of squared residuals indicates a better fit. The two longest ligands (20 and 10 kDa PEG) both show improved fits with the IgE treated as a monovalent receptor and are compared here with those of shorter ligands (750 Da PEG) whose fit is worse with the IgE treated as a monovalent receptor.

affinity could be explained well by a dual mechanism of intramolecular and intermolecular blocking by the PEG moiety (*7*). The low σ values for the ligands with 10 and 20 kDa PEG suggest an analogous steric exclusion effect that would repulse the approach of a second ligand when one ligand is already bound to the IgE.

If the steric blockage due to the high-molecular mass PEG in these ligands is sufficiently substantial to block the approach of a second ligand, then each IgE virtually behaves as a monovalent receptor capable of binding only a single monovalent ligand. To test this idea, we refitted the binding data for the ligands with 10 and 20 kDa PEG, by treating IgE as a monovalent receptor (Figure 1B with σ set to 0). We used the sum of squared residuals (SS) as a metric for the quality of fits to the two models. The results of these alternate fits for the ligands with 10 and 20 kDa PEG are listed in Table 1 along with the alternate fit for one of the shorter ligands (750 Da PEG). We observe that the alternate fits in which the IgE is treated as a monovalent receptor lead to significantly lower SS values, i.e., better fits, for the two longest ligands, whereas for all shorter ligands, including the 5 kDa PEG, the alternate fit is in fact worse than the original fit (data shown for only the ligand with 750 Da PEG). We also note that the effective affinity constants of the two longest ligands from this alternate fit are comparable to the intrinsic affinity of 5×10^7 M^{-1} for the shorter PEG ligands. This is what we would expect if these long ligands were binding primarily in a monovalent fashion to an IgE, as the presence of the long PEG will not affect the initial binding interaction but rather influence the accessibility of the second binding site on the same IgE.

Thus, fits to the binding data for the two longest ligands may be interpreted in either of two ways. In the previous section, we presented evidence for an energetically favorable self-association, between two ligands with a PEG molecular mass of $\geq$5 kDa bound to the same IgE, that stabilizes this conformation. In this section, we present an alternate set of fits that are consistent with a steric exclusion of the second binding site on an IgE when one site is occupied by a ligand with a PEG molecular mass of $\geq$10 kDa. These results, when examined together with the study of Kubetzko et al., suggest that with an increase in the length of the PEG scaffold there is a competition between these two opposing effects. For the 5 kDa PEG, self-association between the PEG tethers enhances the effective affinity. For ligands with a significantly higher PEG molecular mass, the energetically favorable self-association is countered by an entropically driven steric exclusion that attenuates the effective affinity. This is likely the reason for the initial increase followed by a decline in the effective affinity as the PEG molecular mass increases from 2 to 20 kDa (Figure 2A). Data from the simple binding assays that we analyze here are alone not sufficient to resolve the relative contribution of these two effects on the overall affinity, and further mechanistic studies are necessary to improve our understanding of the effect of these two mechanisms on the functional behavior of such PEGylated ligands.

Comparison of the Quality of Fits. It is instructive to examine the quality of the fits to the two models between a short and a long ligand. On the basis of our classification given above, we expect the single-step binding model to provide an adequate fit of the binding data for a short ligand, while for a long ligand, the two-step model will lead to a significantly better fit. To test this prediction, we compared the quality of fits to the two models for 2 and 5 kDa PEG ligands whose solution lengths are close to each other but whose best-fit σ values differ by nearly 10-fold. Moreover, for both these ligands, the PEG tethers are not bulky enough for the steric blockage effect to confound the fits. Figure 3 shows binding titration data for two ligands: MeO−PEG_{2000}−DNP in panels A and B and MeO−PEG_{5000}−DNP in panels C and D. The scatter plots show the fraction of binding sites occupied as a function of the ligand concentration calculated from three independent binding titrations for each ligand. The high apparent affinity of the 5 kDa PEG ligand is obvious from the steeper slope of the titration data and the lower ligand concentration at which the binding sites are saturated in the bottom panel. Such direct visual comparison is possible in this case because the initial IgE concentration was identical for all the experiments that are shown.

The solid curves in each plot are the best fits of the data to either the single-step binding model (Figure 3A,C) or the two-step binding model (Figure 3B,D). As expected, for the 2 kDa PEG ligand, there is very little difference in the quality of the fit between the two models other than a slight improvement in the fit at higher ligand concentrations with the two-step model. In contrast, for the 5 kDa ligand, the two-step binding model offers a noticeably better fit to the experimental data, capturing much more faithfully the steeper profile of the titration curve and the approach to saturation. The residuals, i.e., the difference in the observed fluorescence and the model predicted fluorescence for each titration point, are shown in the inset plots. The residuals in Figure 3C span a range that is nearly twice as large as that in the other three cases, confirming the visual impression that the single-step model provides an inadequate description of the experimental data for this ligand.

Competitive Inhibition of Binding. In the preceding sections, we described a detailed analysis of the equilibrium binding properties of a class of PEGylated monovalent ligands. This analysis relies on data from a direct binding interaction between a ligand and IgE in solution but does not take into account the presence of a competing ligand, such as a multivalent antigen. Generally, it is difficult to model realistically the binding and cross-linking induced by a multivalent antigen because of the large number of possible

Scheme 1: Synthesis of the Fluorescent Hapten DNP-Lys-Flu[a]

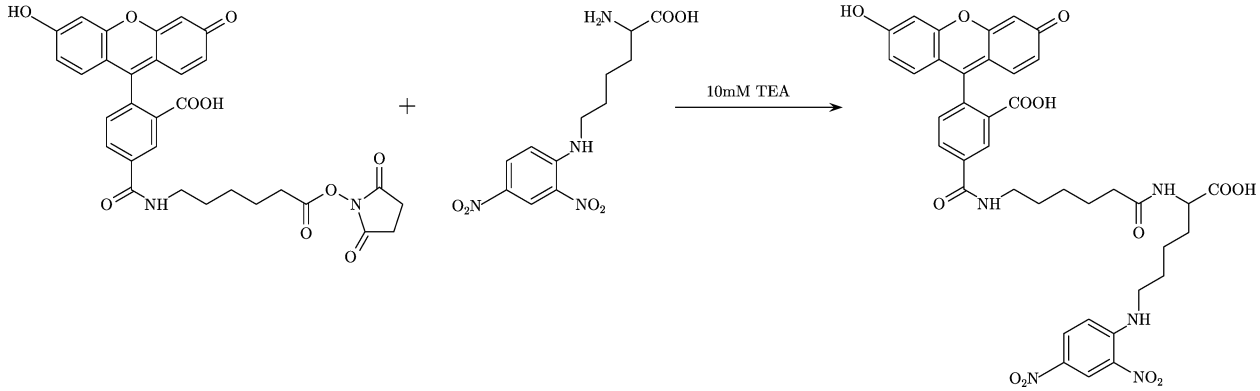

[a] See Materials and Methods for details.

interactions and the complexity of the resulting aggregates, though mathematical simplifications exist for some special cases (*17*, *18*). We tested the capacity of these ligands in an independent competitive binding assay in which the monovalent ligands act as competitive inhibitors of the binding between IgE and a small, high-affinity hapten. A fluorescent label on the small hapten allowed us to distinguish its concentration in the free and IgE-bound forms, and we monitored the fraction of labeled hapten that is displaced from its bound state by a given concentration of a competing monovalent PEG ligand. This indirect competitive inhibition assay serves to approximate the physiological scenario when both a high-avidity multivalent antigen and an inhibitory monovalent ligand are competing for IgE binding sites.

The synthesis and purification of this fluorescent hapten, DNP-Lys-Flu (Scheme 1), are described in Materials and Methods. We found that upon addition of IgE the fluorescence intensity of this hapten increases, and we used the enhancement in fluorescence intensity to monitor its binding to IgE. As illustrated in Figure 4A, a binding titration with anti-DNP IgE showed an excellent fit to a single-step binding model, and the affinity constant of the hapten was determined to be 1.9×10^8 M^{-1}. This value is, within experimental error, identical to the previously reported affinity between DNP-lysine and anti-DNP IgE (*10*). The good fit of the fluorescence intensity data to a single-step binding model indicates that the fluorescence intensity of DNP-Ly-Flu is a good measure of its fraction bound to IgE. The close agreement between the affinity constants of DNP-Lys and DNP-Lys-Flu further suggests that the presence of the fluorescein moiety linked via the seven-atom spacer does not noticeably affect the binding of the fluoresceinated hapten compared to the unlabeled DNP-Lys. We did not investigate the molecular basis for the change in fluorescence intensity upon IgE binding. One possibility is that in the unbound state the conjugated electron systems of the fluorescein and the DNP are interacting with each other to quench the fluorescein fluorescence, and the binding of the DNP group to its IgE binding site relaxes this quenching and enhances the fluorescence intensity.

To standardize the competitive assay and further confirm the validity of using fluorescence intensity as a read-out for the fraction of IgE-bound DNP-Lys-Flu, we used another well-characterized small hapten DCT as the unlabeled competitor and fitted the data to a competitive binding model (Figure 1D). Our objective was to calculate the effective affinity K_I of the unlabeled inhibitor using as a reference the affinity K_X of the labeled hapten determined above. The best-fit value of K_I for DCT from this analysis is 1.3×10^9 M^{-1} which compares well with its affinity constant from a direct binding assay, which was determined to be 1.6×10^9 M^{-1} (*10*). Table 2 lists the best-fit values of the effective affinity (K_I) from this assay for some of the monovalent PEG ligands, and Figure 4B shows representative titration data for DCT and three different monovalent PEG ligands.

Comparing the K_I values listed in Table 2 with the K_{eff} values for the corresponding ligands (Table S1), we observe that ligands with a PEG molecular mass of ≤ 5 kDa are good competitive inhibitors in this assay. For these ligands, the K_I from the competitive binding assay is somewhat higher than the K_{eff} estimated from the direct binding data but follows the same trend. On the other hand, the two longest ligands are poor competitive inhibitors, and the estimates of K_I for these ligands are significantly smaller than their K_{eff} values. This result, while surprising at first glance, can nonetheless be interpreted in the context of a transition from self-association to steric exclusion with an increase in PEG length.

For the 5 kDa PEG ligand, the self-association between the PEG tethers will stabilize the doubly bound state and enhance the likelihood of rebinding if one of the ligands is displaced by a small hapten. In contrast, for ligands with a much longer PEG, we expect the steric exclusion of the second binding site to be most effective in repelling other macromolecules, such as a second ligand or a multivalent antigen, but not necessarily a small hapten. In fact, a small, high-affinity hapten in solution can induce the rapid dissociation of previously bound multivalent antigen and may analogously be able to outcompete a bulky monovalent ligand for the IgE binding sites. In the absence of a second tether, which exists for the 5 kDa PEG ligand, there is no enhanced probability of rebinding for the higher-molecular mass ligands. Moreover, the probability of rebinding for these long PEG ligands may be even further diminished because of an intramolecular blocking mechanism, as postulated by Kubetzko et al. (*7*), in which the bulky PEG tether tends to block the approach of the antigenic epitope on the ligand to its binding pocket.

Equilibrium Binding of Bivalent PEG Ligands to IgE in Solution. Baird et al. (*4*) previously observed two distinct categories of inhibitory capacity with bivalent (i.e., DNP−PEG_x−DNP) ligands. As shown in Figure 5A, ligands with

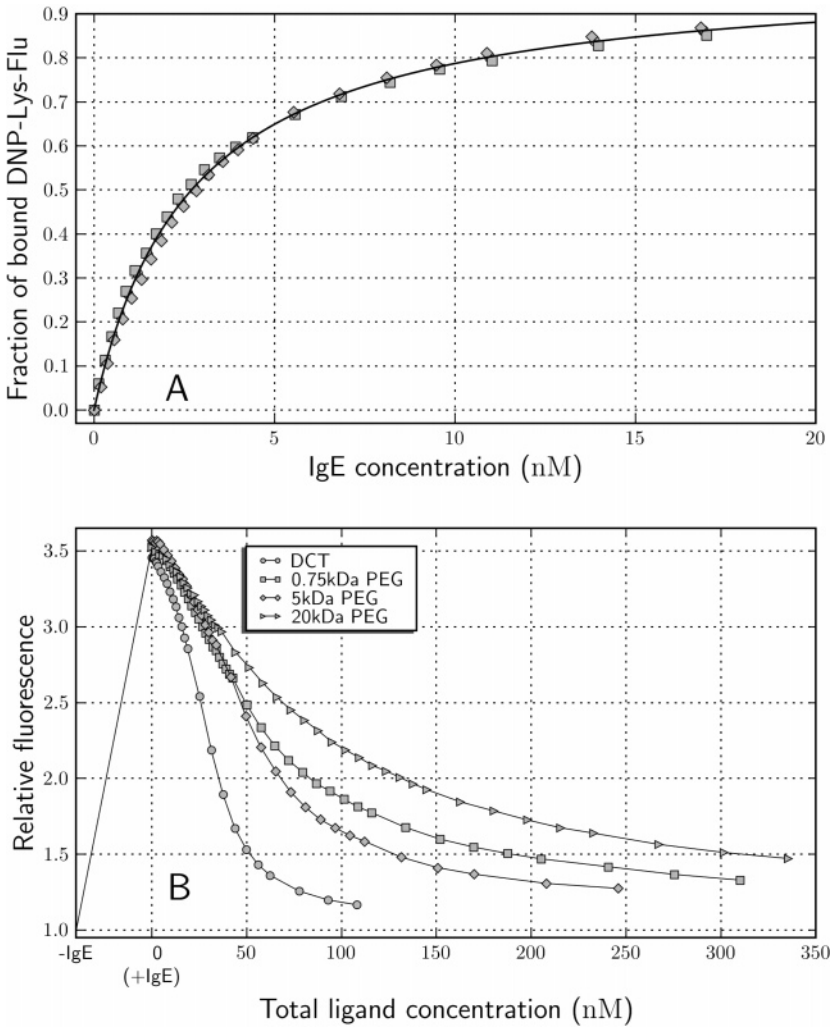

FIGURE 4: Binding characteristics of DNP-Lys-Flu and its use as a fluorescent hapten in a competitive binding assay. (A) Direct binding titration between the hapten DNP-Lys-Flu and anti-DNP IgE. The scatter plots show experimental data from three independent titrations, and the solid line is the simultaneous fit of the three experiments to a single-step binding model. The change in the fluorescence intensity of DNP-Lys-Flu upon IgE binding was used to determine its fraction bound to IgE (eq 1). The best-fit value of the affinity K_X of the hapten was calculated to be 1.9×10^8 M^{-1} from this fit. (B) Representative titration data from the competitive binding assay for DCT and a short (750 Da PEG), intermediate (5 kDa PEG), and long (20 kDa PEG) monovalent PEG ligand. The fluorescence intensity of DNP-Lys-Flu is plotted as a function of increasing ligand concentration and is normalized to the fluorescence of DNP-Lys-Flu alone prior to the addition of IgE or the competitive binder. The DNP-Lys-Flu concentration was 18.5 nM at the start of the titration, and anti-DNP IgE was added to a final concentration of ~20 nM.

Table 2: Best-Fit Values of the Effective Affinity (K_I) for Some Monovalent Ligands When They Inhibit the Binding of the Small Fluorescent Hapten DNP-Lys-Flu[a]

ligand	K_I ($\times 10^9$ M^{-1})	ligand	K_I ($\times 10^9$ M^{-1})
DCT	1.3 ± 0.614	$MPEG_{5000}$−DNP	0.23 ± 0.007
$MPEG_{750}$−DNP	0.18 ± 0.014	$MPEG_{10000}$−DNP	0.13 ± 0.005
$MPEG_{2000}$−DNP	0.16 ± 0.015	$MPEG_{20000}$−DNP	0.096 ± 0.002

[a] The affinity of DCT has been previously determined to be 1.6×10^9 M^{-1} from direct binding data (*10*). The effective affinities of the monovalent PEG ligands from direct binding data are listed in Table S1. The best-fit values shown here were obtained by simultaneously fitting three independent experiments, and the error range is the standard deviation of best-fit values from fitting individual experiments.

3.35, 8, and 10 kDa PEG are all very similar in their inhibitory capacity with IC_{50} values around 10 nM. In contrast, the ligands with 0.4 and 1 kDa PEG spacers were more modest inhibitors with IC_{50} values of ≥50 nM. To investigate this distinction, we analyzed the data from equilibrium binding titrations of these ligands with IgE in solution. A preliminary fit of the binding data to a single-step binding model (Figure 1A) indicates that the IC_{50} values are well-correlated with the effective affinity (K_{eff}) of these ligands for IgE. DNP−PEG_{3350}−DNP is roughly 8 times more potent as an inhibitor than DNP−PEG_{1000}−DNP, and as shown in Table 3, K_{eff} for the DNP−PEG_{3350}−DNP is ~8 times greater than K_{eff} for DNP−PEG_{1000}−DNP. A comparison of the experimental binding data for the two ligands is shown in Figure 5B with the best-fit binding curves.

We reasoned that the high inhibitory capacity of the bivalent ligands is due to their propensity to form stable intramolecular cross-links in which the two ends of a bivalent ligand are bound to adjacent binding sites on the same IgE. Formation of productive intramolecular cross-links is expected to enhance the inhibition to binding by a multivalent antigen, because the dissociation of one end from an IgE binding site will more likely lead to rebinding if the other end is tethered to the same IgE. To test whether solution binding data are consistent with this hypothesis, we refitted them to a bivalent binding model that includes an intramo-

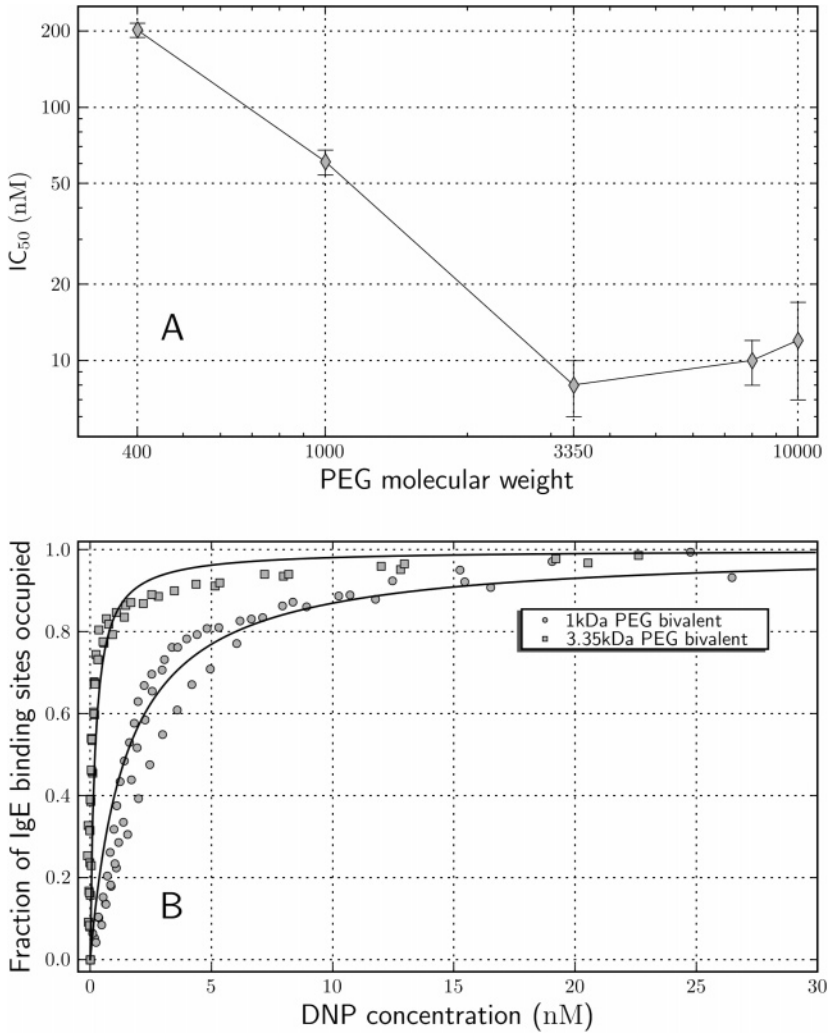

FIGURE 5: Inhibition and binding characteristics of bivalent ligands. (A) IC_{50} values (±standard deviation from three or more independent inhibition experiments) of bivalent ligands as a function of the PEG molecular mass (data from ref *4*). (B) Equilibrium binding data for two different bivalent ligands, the moderate inhibitor DNP−PEG_{1000}−DNP and the strong inhibitor DNP−PEG_{3350}−DNP. Scatter plots show binding data from from three independent titrations for each ligand. The solid lines are the best-fit curves from fitting to a single-step model (Figure 1a) with the effective affinity constants listed in Table 3. The total IgE concentration for each titration was 3.2 nM prior to any ligand addition.

Table 3: Best-Fit Values of the Effective Affinity Constant (K_{eff}) and the Intramolecular Cross-Linking Constant (J) (from fitting solution binding data) for Bivalent Ligands and Their IC_{50} Values (for inhibition of degranulation)[a]

ligand	K_{eff} ($\times 10^9$ M^{-1})	J	IC_{50} (nM)
DNP−PEG_{1000}−DNP	0.667 (0.547, 0.756)	11.3 (4.07, 37.9)	61 ± 7
DNP−PEG_{3350}−DNP	5.12 (4.30, 6.78)	100.3 (16.7, 511)	8 ± 2
DNP−PEG_{10000}−DNP	15.2 (9.48, 42.5)	301.3 (32.0, 1630)	10 ± 2

[a] K_{eff} is the effective affinity for the interaction between a DNP group and the binding site on an IgE. Values of J shown here were determined from fits with K fixed at 5×10^7 M^{-1}. For each ligand, data from three independent experiments were simultaneously fit. The best-fit parameter value along with a 95% confidence interval from fitting 200 bootstrap simulations drawn from the experimental data is shown for each ligand. The IC_{50} values were taken from ref *4*.

lecularly cross-linked state (Figure 1C). As described in the Appendix, the relevant equilibrium constants that appear as parameters in this model are the intrinsic affinity K for the initial binding and an intramolecular cross-linking constant J. For these fits, we fixed the intrinsic affinity K at 5×10^7 M^{-1}, the consensus value from the fits of binding data for monovalent ligands with comparable PEG lengths.

The values for the cross-linking constant obtained from the fits are shown in Table 3; we observe that J is ∼9 times greater for DNP−PEG_{3350}−DNP than for DNP−PEG_{1000}−DNP. This difference in the intramolecular cross-linking constant mirrors the observed difference in the IC_{50} values of these ligands. There is a smaller relative increase of ∼3-fold in J for DNP−PEG_{10000}−DNP compared to DNP−PEG_{3350}−DNP but no significant difference in the inhibitory capacity of these two ligands. It is likely that for these high values of J the equilibrium binding is shifted toward exclusive formation of intramolecular cross-links, and kinetic, rather than thermodynamic, differences between a multivalent antigen and a bivalent ligand interacting with the cell surface receptor dictate the degranulation response.

Another putative mechanism for the inhibitory action of the bivalent PEG ligands would be the formation of stable cyclic dimers that fail to initiate degranulation, such as those observed with the bivalent ligand $(DCT)_2$-cys (*19*). However, gel permeation chromatography data show no evidence for any higher-molecular mass species, allowing us to neglect the formation of cyclic dimers in our binding analysis in solution (*4*). It is conceivable that such complexes could form

on the cell surface because of the high local density of IgE receptor complexes. It has been proposed that under conditions of high cell surface density of receptors coupled with high occupancy of binding sites, even small nonspecific binding interactions could potentially trigger receptor aggregation (*20*). Furthermore, bivalent ligands such as $(DCT)_2$-cys which efficiently form cyclic dimers at low concentrations that are optimal for binding typically stimulate limited degranulation at higher ligand concentrations where inter-IgE cross-linking occurs (*19*, *21*). However, the failure of bivalent PEG ligands to induce any degranulation over a range of concentrations spanning 4 orders of magnitude (*4*) makes such intermolecular cross-linking and receptor aggregation by these ligands at the cell surface a highly improbable event.

The propensity of these bivalent PEG ligands to form stable intramolecular cross-links is similar to that observed by Schweitzer-Stenner et al. for another class of DNP dimers (*22*). In that study, the authors found that rigid oligoproline-linked DNP dimers with spacer lengths in the range of 130−150 Å almost exclusively form intramolecular cross-links with anti-DNP IgE. The solution lengths of the PEG-linked dimers examined here are shorter than the length of the rigid oligoproline spacers in that study. However, the PEG linkers are considerably more flexible and can assume a somewhat extended conformation if the entropic loss in the process is sufficiently offset by the enthalpic gain due to the formation of a stable intramolecular cross-link. Moreover, a recent study utilizing photoinduced electron transfer (PET) to probe polyproline structure presented evidence for significant structural heterogeneity in polyprolines (*23*). In particular, these authors concluded that average end-to-end distances of polyprolines are significantly reduced compared to theoretical predictions, most likely because of interspersed cis isomers. Thus, end-to-end distances of the apparently rigid oligoproline ligands may, in fact, be comparable to those of the flexible PEG ligands examined here.

We note that for these bivalent ligands the model with intramolecular cross-linking (Figure 1C) offers no enhancement in the quality of fits compared to the single-step model with a single effective affinity (Figure 1A). This lack of improvement in the fits for bivalent ligands is also reflected in the wide confidence intervals (Table 3) for the best-fit values of the intramolecular cross-linking constant. Thus, while the intramolecular cross-linking model offers a physically intuitive basis for understanding the differences in the effective affinities between bivalent ligands of different lengths, it does not further refine the simple correlation between a high effective affinity and a high inhibitory capacity.

DISCUSSION

In this study, we systematically characterized the equilibrium binding interactions between a class of PEGylated monovalent and bivalent DNP-functionalized ligands and anti-DNP IgE in solution. These ligands are biologically relevant because of their previously reported inhibitory potential against multivalent antigen-induced degranulation in RBL-2H3 mast cells (*4*). A detailed analysis of the binding interaction is necessary because relatively subtle changes in ligand structures can have profound effects on the nature of conjugates they form with cell surface receptors and the physiological outcome of that interaction (*24*). Here we have shown that simply varying the length of the PEG scaffold significantly modulates the binding characteristics of these ligands. We used a well-established fluorescence assay to characterize the ligand−IgE binding interaction and first fitted the binding data to a simple single-step binding model (Figure 1A). We established the effective affinity, K_{eff}, of each ligand for IgE and observed a dependence of the effective affinity on the PEG molecular mass (Figure 2A) that could not be explained simply on the basis of the interaction between the antibody binding site and the antigenic epitope on the ligand.

The single-step binding model assumes that two monovalent ligands bind to an IgE receptor in a manner independent of each other and with identical affinity. This model is an adequate physical description of the binding for small ligands such as DCT as well as some macromolecular ligands such as ds-DNA-DNP whose interaction with IgE is primarily governed by the binding of the antigenic epitope (DNP + linker) on the ligand to the IgE binding site. In particular, for the ds-DNA-DNP ligands, the length of the dsDNA appears to have a negligible effect on the overall binding affinity (*14*). In contrast, the effective binding affinity of the PEGylated DNP ligands is significantly affected by the length of the PEG tether, which is evident from the 10-fold difference in effective affinities of ligands with 2 and 10 kDa PEG (Figure 2A).

We therefore fit the binding data to a more realistic two-step binding model (Figure 1B) that allowed us to dissect the binding interaction and gain better insight into the role played by the PEG scaffold. This two-step binding model was introduced to resolve the contribution of the PEG scaffolds to the effective affinity, because it decouples the intrinsic affinity of the antigenic epitope from interactions between PEG scaffolds of two ligands bound to the same IgE. The single-step binding model (Figure 1A) is a special case of the two-step binding model (Figure 1B) when $\sigma = 1$. On the basis of our fits with this two-step model (Figure 2), we propose an energetically favorable configuration characterized by a high value of the interaction term σ when two monovalent ligands with a PEG molecular mass in the 5−10 kDa range are bound to the same IgE. This stabilization may be mediated by self-association of the PEG scaffolds on the two ligands when they are tethered close together (∼100 Å separation). We also tested the binding between the monovalent Fab′ fragment and long PEG ligands and concluded that this enhanced stabilization cannot be explained simply by a nonspecific binding of the PEG tail to IgE. For ligands with a PEG molecular mass of ≳10 kDa, the bulk of the PEG sterically blocks the second binding site on a singly occupied IgE.

We also developed a competitive binding assay which tested these monovalent ligands as competitive inhibitors of the binding of a small fluorescent hapten to IgE. This assay was designed to test the inhibitory potential of these ligands in a simplified and mathematically tractable scenario. Fits to the competitive binding data are consistent with the hypothesis that there is an energetic stabilization for intermediate-length PEG whereas steric blockage occurs for longer PEG ligands.

Finally, we described the binding of bivalent ligands with a model that quantifies their propensity to form stable, nonstimulatory intramolecular cross-links. Fitting the solution binding data for bivalent ligands to this model confirmed that the capacity to form effective intramolecular cross-links is governed by the length of the PEG spacer and that this is a good determinant of the inhibitory capacity of these ligands. Our results shed light on the spectrum of behavior displayed by PEG-linked ligands, and we anticipate that such considerations will influence the selection and design of PEG scaffolds for similar biological applications.

APPENDIX: BINDING MODELS

The equations used for fitting the direct binding and competitive binding data are derived below. For each model, we express the fraction of binding sites occupied as a function of known total concentrations of receptor and ligand. The general theory for binding of bivalent ligands was described by Dembo and Goldstein (*25*), and we have adapted specific features from their more general analysis.

Single-Step Binding Model: Monovalent Binding with a Single Effective Affinity Constant K_{eff}. This model is the simplest single-step binding reaction between a binding site $\mathcal{S}$ and a monovalent ligand $\mathcal{L}$

$$\mathcal{S} + \mathcal{L} \overset{K_{\text{eff}}}{\rightleftharpoons} \mathcal{SL}$$

schematically illustrated in Figure 1A. In this model, the two binding sites on an IgE are assumed to be independent and of identical affinity with an affinity constant K_{eff}. The concentration of bound sites is

$$B = K_{\text{eff}} SL \tag{2}$$

where S and L are the free (unbound) site and ligand concentrations, respectively. Using conservation laws for the total site concentration (S_T) and total ligand concentration (L_T), the fraction of binding sites occupied (f) is shown to be

$$f = B/S_T = \frac{1 + K_{\text{eff}}(S_T + L_T) - \sqrt{[1 + K_{\text{eff}}(S_T + L_T)]^2 - 4K_{\text{eff}}{}^2 S_T L_T}}{2K_{\text{eff}} S_T} \tag{3}$$

Two-Step Binding Model: Monovalent Binding with an Affinity Constant K and an Interaction Coefficient σ. This model is schematically shown in Figure 1B. A bivalent receptor $\mathcal{R}$ binds two monovalent ligands $\mathcal{L}$ sequentially forming first a singly bound form ($\mathcal{RL}$) followed by a doubly bound form ($\mathcal{RL}_2$).

$$\mathcal{R} + \mathcal{L} \overset{2K}{\rightleftharpoons} \mathcal{RL} \overset{\sigma K/2}{\rightleftharpoons} \mathcal{RL}_2$$

The intrinsic affinity constants of the two binding steps are K and σK, respectively, and the multiplicative factors of 2 and $^1/_2$ arise from the bivalency of the receptor. The first binding event can occur with equal likelihood at either of the two sites on the receptor, and a ligand can dissociate from a doubly bound receptor at either of the two sites. The ratio σ is a measure of how the presence of the first ligand on a singly bound receptor affects the binding at the second site. A σ of >1 indicates that the binding of a second ligand to a singly bound receptor is preferred, indicating a positive cooperative effect. A σ of <1 implies that the binding of a second ligand is disfavored, indicating a steric blockage of the second binding site.

Concentrations of the various species are defined as

$$R = [\mathcal{R}]L = [\mathcal{L}]B_1 = [\mathcal{RL}] \tag{4}$$

$$R_T = [\mathcal{R}]_T L_T = [\mathcal{L}]_T B_2 = [\mathcal{RL}_2] \tag{5}$$

where R and L are the free receptor and free ligand concentrations, respectively, and R_T and L_T are the total receptor and total ligand concentrations, respectively. By definition, $B_1 = 2KRL$ and $B_2 = \sigma K^2 RL^2$, which lead to the following conservation laws for total receptor and total ligand concentration, respectively:

$$R_T = R[1 + KL(2 + \sigma KL)] \tag{6}$$

$$L_T = L + \frac{2KR_T L(1 + \sigma KL)}{1 + KL(2 + \sigma KL)} \tag{7}$$

Equation 7 is a cubic equation in L that we solve numerically with the physical constraint $0 \le L \le L_T$ to determine L for given values of L_T, R_T, K, and σ. Having solved for L, we find the fraction of receptor binding sites that are occupied (bound to a ligand) is given by

$$f = (B_1 + 2B_2)/(2R_T) = \frac{KL(1 + \sigma KL)}{1 + KL(2 + \sigma KL)} \tag{8}$$

We also note that after substitution of $\sigma = 1$, eq 8 assumes the form

$$f = \frac{KL}{1 + KL} \tag{9}$$

This equation is a familiar hyperbolic saturation curve for the interaction between a monovalent receptor and a monovalent ligand that bind each other with an affinity K, implying that the single-step binding model is a special case of the two-step binding model in which $\sigma = 1$.

Bivalent Binding Model: Bivalent Binding with an Affinity Constant K and a Cross-Linking Constant J. In this model shown schematically in Figure 1C, we take into account the possibility of intramolecular cross-linking when a bivalent ligand $\mathcal{L}$ binds to a bivalent receptor $\mathcal{R}$. The ligand first binds at one of the receptor binding sites with an intrinsic affinity K, forming a singly bound receptor $\mathcal{RL}$ which then isomerizes with an equilibrium constant (cross-linking constant) J to an intramolecularly cross-linked state $\mathcal{RL}'$. That is

$$\mathcal{R} + \mathcal{L} \overset{4K}{\rightleftharpoons} \mathcal{RL} \overset{J/2}{\rightleftharpoons} \mathcal{RL}'$$

As before, we define the concentrations of the various species as

$$R = [\mathcal{R}]L = [\mathcal{L}]B_1 = [\mathcal{RL}]$$

$$R_T = [\mathcal{R}]_T L_T = [\mathcal{L}]_T B_2 = [\mathcal{RL}'] \tag{10}$$

The concentrations of the two bound forms are as follows: $B_1 = 4KRL$ and $B_2 = 2JKRL$. With the relation $B = B_1 + B_2 = 2K(2 + J)RL$, the conservation equations for total receptor and total ligand concentrations are

$$R_T = R + B \tag{11}$$

$$L_T = L + B \tag{12}$$

As before, we solve for B

$$B = \frac{1}{2K'}\{1 + K'(R_T + L_T) - \sqrt{[1 + K'(R_T + L_T)]^2 - 4K'^2 S_T L_T}\} \tag{13}$$

where $K' = 2K(2 + J)$. The fraction of receptor binding sites that are occupied is given by

$$f = (B_1 + 2B_2)/2R_T = \frac{1 + J}{2 + J}\frac{B}{R_T} \tag{14}$$

Competitive Binding Model: Inhibition of Monovalent Binding with a Small Fluorescent Hapten. As shown in Figure 1D, a small hapten $\mathcal{X}$ and a monovalent ligand $\mathcal{I}$ both compete for a monovalent receptor $\mathcal{J}$ (the binding site on an IgE) with different affinity constants K_X and K_I, respectively.

$$\mathcal{JI} \overset{K_I}{\rightleftharpoons} \mathcal{J} \overset{K_X}{\rightleftharpoons} \mathcal{JX}$$

There are three different unbound species and two bound species whose concentrations are defined as

$$S = [\mathcal{J}]X = [\mathcal{X}]I = [\mathcal{I}]B_X = [\mathcal{JX}]$$

$$S_T = [\mathcal{J}]_T X_T = [\mathcal{X}]_T I_T = [\mathcal{I}]_T B_I = [\mathcal{JI}] \tag{15}$$

The concentrations of bound hapten and bound inhibitor are as follows: $B_X = K_X SX$ and $B_I = K_I SI$, respectively. There are now three conservation equtions for total receptor, hapten, and inhibitor concentrations:

$$S_T = S(1 + K_X X + K_I I) \tag{16}$$

$$X_T = X + K_X SX \tag{17}$$

$$I_T = I + K_I SI \tag{18}$$

From eq 16, we have

$$S = S_T/(1 + K_X X + K_I I) \tag{19}$$

and substituting for S in eqs 17 and 18, we rewrite them as

$$X + \frac{K_X X S_T}{1 + K_X X + K_I I} = X_T \tag{20}$$

$$I + \frac{K_I I S_T}{1 + K_X X + K_I I} = I_T \tag{21}$$

Equations 20 and 21 may be numerically solved as a system of coupled equations with the additional constraints $0 \le X \le X_T$ and $0 \le I \le I_T$ to determine the free hapten concentration X and the free inhibitor concentration I for given total concentrations X_T, I_T, and S_T. We are interested in the ratio of bound hapten concentration to total hapten concentration which is then given by

$$f' = B_X/X_T = \frac{K_X X S_T}{X_T(1 + K_X X + K_I I)} \tag{22}$$

SUPPORTING INFORMATION AVAILABLE

Physical characteristics, yields, and ^{1}H NMR spectral information are included for the 10 and 20 kDa PEG monovalent ligands. We analyze the binding of 5 and 10 kDa PEG monovalent ligand to monovalent Fab′ fragments to estimate the degree of nonspecific interaction between the PEG tail and Fab′. We also describe in detail our data fitting procedure. Table S1 lists the bootstrap confidence intervals for parameters estimated from fitting the monovalent ligand binding data, as well as the estimated PEG lengths for the range of PEG molecular masses that were examined. This material is available free of charge via the Internet at http://pubs.acs.org.

REFERENCES

1. Mammen, M., Choi, S. K., and Whitesides, G. M. (1998) Polyvalent Interactions in Biological Systems: Implications for Design and Use of Multivalent Ligands and Inhibitors, *Angew. Chem., Int. Ed. 37* (20), 2754−2794.
2. Kinet, J. P. (1999) The high-affinity IgE receptor (FcϵRI): From physiology to pathology, *Annu. Rev. Immunol. 17*, 931−972.
3. MacGlashan, D., Jr., and Lichtenstein, L. M. (1983) Studies of antigen binding on human basophils. I. Antigen binding and functional consequences, *J. Immunol. 130* (5), 2330−2336.
4. Baird, E. J., Holowka, D., Coates, G. W., and Baird, B. (2003) Highly effective poly(ethylene glycol) architectures for specific inhibition of immune receptor activation, *Biochemistry 42* (44), 12739−12748.
5. Zalipsky, S., and Harris, J. M. (1997) Introduction to Chemistry and Biological Applications of Poly(ethylene glycol), in *Poly-(ethylene glycol) Chemistry and Biological Applications* (Harris, J. M., and Zalipsky, S., Eds.) Chapter 1, pp 1−13, American Chemical Society, Washington, DC.
6. Lasic, D. (1997) The Conformation of Polymers at Interfaces, in *Poly(ethylene glycol) Chemistry and Biological Applications* (Harris, J. M., and Zalipsky, S., Eds.) Chapter 3, pp 31−44, American Chemical Society, Washington, DC.
7. Kubetzko, S., Sarkar, C. A., and Pluckthun, A. (2005) Protein PEGylation decreases observed target association rates via a dual blocking mechanism, *Mol. Pharmacol. 68* (5), 1439−1454.
8. Kramer, R. H., and Karpen, J. W. (1998) Spanning binding sites on allosteric proteins with polymer-linked ligand dimers, *Nature 395* (6703), 710−713.
9. Subramanian, K., Holowka, D., Baird, B., and Goldstein, B. (1996) The Fc segment of IgE influences the kinetics of dissociation of a symmetrical bivalent ligand from cyclic dimeric complexes, *Biochemistry 35* (17), 5518−5527.
10. Erickson, J., Kane, P., Goldstein, B., Holowka, D., and Baird, B. (1986) Cross-linking of IgE-receptor complexes at the cell surface: A fluorescence method for studying the binding of monovalent and bivalent haptens to IgE, *Mol. Immunol. 23* (7), 769−781.
11. Efron, B., and Tibshirani, R. J. (1994) *An Introduction to Bootstrap*, Chapman and Hall, London.
12. Lakowicz, J. (1983) *Principles of Fluorescence Spectroscopy*, Chapter 5, pp 111−153, Plenum Press, New York.
13. Baird, B., Zheng, Y., and Holowka, D. (1993) Structural mapping of IgE-Fc-ϵ-RI, an immunoreceptor complex, *Acc. Chem. Res. 26* (8), 428−434.

14. Paar, J. M., Harris, N. T., Holowka, D., and Baird, B. (2002) Bivalent ligands with rigid double-stranded DNA spacers reveal structural constraints on signaling by FcεRI, *J. Immunol. 169* (2), 856−864.
15. Efremova, N. V., Sheth, S. R., and Leckband, D. E. (2001) Protein-Induced Changes in Poly(ethylene glycol) Brushes: Molecular Weight and Temperature Dependence, *Langmuir 17* (24), 7628−7636.
16. Zheng, Y., Shopes, B., Holowka, D., and Baird, B. (1992) Dynamic conformations compared for IgE and IgG1 in solution and bound to receptors. *Biochemistry 31* (33), 7446−7456.
17. Perelson, A. S. (1984) Some Mathematical Models of Receptor Clustering by Multivalent Antigen, in *Cell Surface Dynamics* (Perelson, A. S., DeLisi, C., and Wiegel, F. W., Eds.) Chapter 9, pp 223−276, Marcel Dekker, New York.
18. Xu, K., Goldstein, B., Holowka, D., and Baird, B. (1998) Kinetics of multivalent antigen DNP-BSA binding to IgE-FcεRI in relationship to the stimulated tyrosine phosphorylation of FcεRI, *J. Immunol. 160* (7), 3225−3235.
19. Posner, R. G., Subramanian, K., Goldstein, B., Thomas, J., Feder, T., Holowka, D., and Baird, B. (1995) Simultaneous cross-linking by two nontriggering bivalent ligands causes synergistic signaling of IgE Fc epsilon RI complexes, *J. Immunol. 155* (7), 3601−3609.
20. Schweitzer-Stenner, R., and Pecht, I. (2005) Death of a dogma or enforcing the artificial: Monomeric IgE binding may initiate mast cell response by inducing its receptor aggregation, *J. Immunol. 174* (8), 4461−4464.
21. Harris, N. T., Goldstein, B., Holowka, D., and Baird, B. (1997) Altered patterns of tyrosine phosphorylation and Syk activation for sterically restricted cyclic dimers of IgE-FcεRI, *Biochemistry 36* (8), 2237−2242.
22. Schweitzer-Stenner, R., Licht, A., Luscher, I., and Pecht, I. (1987) Oligomerization and ring closure of immunoglobulin E class antibodies by divalent haptens, *Biochemistry 26* (12), 3602−3612.
23. Doose, S., Neuweiler, H., Barsch, H., and Sauer, M. (2007) Probing polyproline structure and dynamics by photoinduced electron transfer provides evidence for deviations from a regular polyproline type II helix, *Proc. Natl. Acad. Sci. U.S.A. 104* (44), 17400−17405.
24. Holowka, D., and Baird, B. (1996) Antigen-mediated IgE receptor aggregation and signaling: A window on cell surface structure and dynamics, *Annu. Rev. Biophys. Biomol. Struct. 25*, 79−112.
25. Dembo, M., and Goldstein, B. (1978) Theory of equilibrium binding of symmetric bivalent haptens to cell surface antibody: Application to histamine release from basophils, *J. Immunol. 121* (1), 345−353.

BI702094J